THOMAS J. KISTENMACHER

EFFECTS OF CHEMICAL SUBSTITUTION ON THE STRUCTURAL AND SUPERCONDUCTING PROPERTIES OF SOME HIGH-CRITICAL-TEMPERATURE COPPER OXIDE CERAMICS

The recently discovered high-critical-temperature (T_c) copper oxide superconductors continue to draw considerable research effort, and one aspect of this endeavor centers on the effect of chemical substitution on structure and superconductivity. Herein, some of the effects of chemical substitution on these properties for the superconductors $La_{2-t}A_t(Cu_{1-x}M_x)O_z$ (LSCO, where A is typically Ba or Sr; $t \approx 0.2$; $z \approx 4$; $T_c \approx 40$ K at $x = 0$; and M is a divalent or trivalent dopant ion) and $YBa_2(Cu_{1-x}M_x)_3O_y$ (YBCO, where $y \approx 7$, and $T_c \approx 90$ K at $x = 0$) are presented and analyzed. Two specific topics are addressed: (1) the nature and magnitude of the effects of substitution of magnetic and nonmagnetic rare-earth ions for La^{3+} in the LSCO ceramics and for Y^{3+} in the YBCO ceramics; and (2) the complexity, comparability, and consequences of chemical doping at the copper sites in both families. Because of the chemical and structural intricacies of these materials, these studies are considerably more complex to undertake experimentally, more difficult to analyze quantitatively, and more demanding theoretically than chemically and structurally simpler systems.

INTRODUCTION

One way in which the recently discovered[1,2] high-critical-temperature (T_c) copper oxide superconductors differ from their predecessors is in their degree of chemical and structural complexity. Earlier, lower-T_c (<22 K) elemental and compound superconductors generally adopted simple close-packed or well-recognized crystalline structures. The structural simplicity of these earlier materials is illustrated, for example, by the elemental superconductor Nb ($T_c \approx 9$ K), which assumes a body-centered cubic arrangement, whereas the superconducting cubic phase of NbN ($T_c \approx 15$ K) adopts the NaCl (face-centered cubic) motif. In addition, except for the possibility of nonstoichiometry (viz., NbN_x, where $x < 1$) or isotopic substitution, these examples underscore the rudimentary chemical versatility of earlier known superconductors. In contrast, even the empirical chemical formulations of the first two high-temperature copper oxide superconductors $La_{2-t}A_t(Cu_{1-x}M_x)O_z$ (LSCO, where A is typically Ba or Sr; $t \approx 0.2$; $z \approx 4$; $T_c \approx 40$ K at $x = 0$; and M is a divalent dopant ion such as Zn^{2+} or Ni^{2+} or a trivalent dopant ion such as Al^{3+} or Ga^{3+}) and $YBa_2(Cu_{1-x}M_x)_3O_y$ (YBCO, where $y \approx 7$; $T_c \approx 90$ K at $x = 0$; and M is as above) underscore their structural and electronic complexity.

Continuing in this vein, and given the prominent position of crystal structure in the attainment of superconductivity in these two families of copper oxide ceramics, the basic architecture of their crystal structures will be illustrated and discussed in some detail. The higher symmetry (body-centered tetragonal) and simpler crystalline motif (Fig. 1; Table 1; see, e.g., Ref. 3) adopted by the LSCO ceramics are based on those of the stoichiometric parent compound La_2CuO_4, which is an insulator. The principal structural elements of interest (Figs. 1 and 2) in the La_2CuO_4 motif are sheets of nine-coordinate La^{3+} sites separating planes of vertex-sharing octahedral Cu^{2+} sites.

Moreover, it follows from the empirical formula of the LSCO ceramics that substitution at the lanthanum ion site by an alkaline earth ion and creation of electron holes are crucial in achieving both conductivity and superconductivity. In fact, substitution of about 20% of the Sr^{2+} (or Ba^{2+}) ions at the La^{3+} sites leads to an optimized critical temperature near 40 K. The nature of the electronic holes generated in the CuO_6 plane has, however, been a point of some contention. In a pure ionic-bonding limit, these holes could be (1) generated at the Cu atom site, leading to Cu^{2+}/Cu^{3+} mixed valency; or (2) created at the oxygen atom site, yielding an electronic charge slightly less in magnitude than −2 (as appropriate to the parent La_2CuO_4 compound). Important to what follows, however, is that the relative simplicity of this structural motif and the small number of sites available for substitution suggest that the effects of doping on structural properties and critical temperature should, in principle, be chemically and experimentally uncomplicated.

In the lower symmetry (primitive orthorhombic) and more elaborate crystalline structure (Fig. 3; Table 2; see,

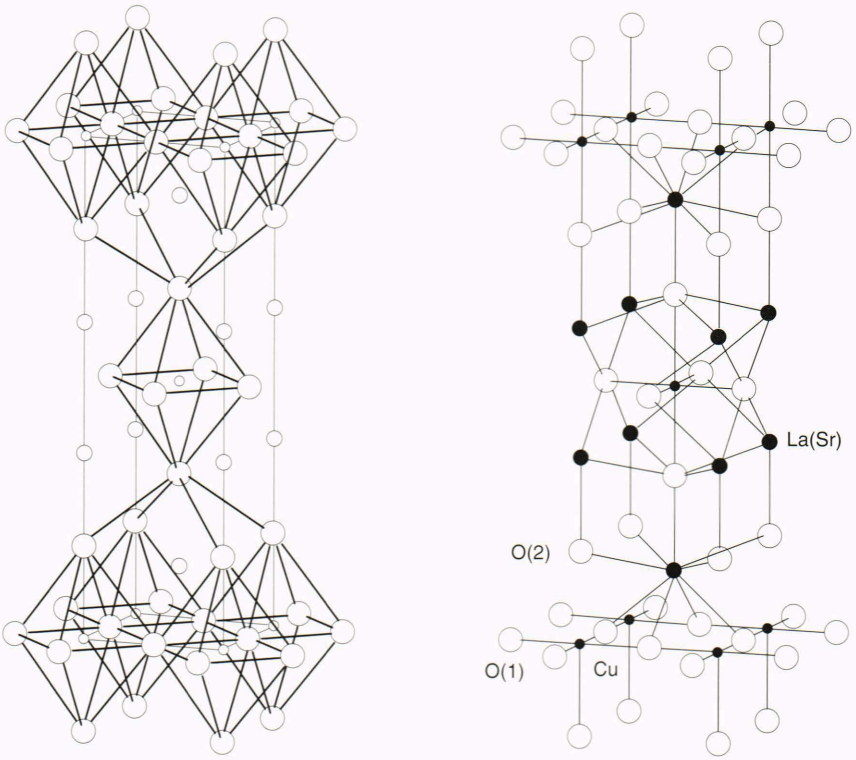

Figure 1. Illustrations of the tetragonal crystal structure of the LSCO ceramics, for example, $La(Sr)_2CuO_4$. Here, the crystallographic *c* axis is vertical.

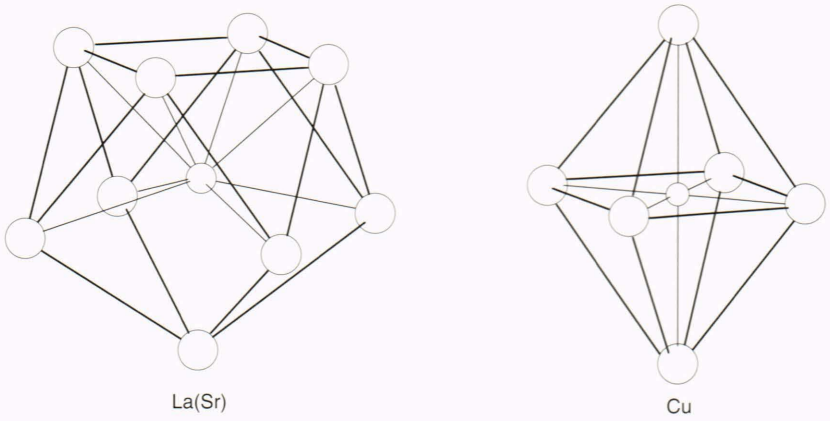

Figure 2. Coordination geometry about the La(Sr) and Cu ion sites in the LSCO ceramics, for example, $La(Sr)_2CuO_4$.

Table 1. Atomic coordinates and site symmetries for La_2CuO_4 in space group I4/m mm.

Atom	Wyckoff notation	Site symmetry	Atomic position
La	4e	4mm (C_{4v})	0, 0, ≈1/3
Cu	2a	4/m mm (D_{4h})	0, 0, 0
O(1)	4c	mmm (D_{2h})	0, 1/2, 0
O(2)	4e	4mm (C_{4v})	0, 0, ≈1/5

e.g., Refs. 4 and 5) adopted by the YBCO ceramics, a single site for the pseudo–rare earth (Y^{3+}) or lanthanide ion and two symmetry-related, ten-coordinate sites for the alkaline earth (Ba^{2+}) ions are seen (Figs. 3 and 4). The complexity in the interpretation of the substitution results for the Y^{3+} ion is then expected to be similar to that for the LSCO ceramics.

An added complication in the YBCO ceramics, however, is that two classes (viz., Figs. 3 and 4) of copper sites are available for substitution: (1) two symmetry-related planes of CuO_5 edge-shared square pyramids—Cu(2) sites; and (2) a symmetry-independent layer containing chains of CuO_4 polyhedra exhibiting near–square-planar geometry—Cu(1) sites. Even in this native ceramic, a formal electron count (holding, as above, the rare earth and alkaline earth ions to ideal ionic charges of +3 and +2, respectively) requires that holes (1) be generated at either or both copper sites, with the rudimentary scenario being Cu^{2+} ions at the two Cu(2) sites per cell and a Cu^{3+} ion at the lone Cu(3) site; or (2) be created at the oxygen site, yielding an oxygen ion charge slightly less in magnitude than −2 (−1.86*e*, in fact). Finally, the complication of having two copper sites available for substitution has made interpretation of the effects of metal doping for

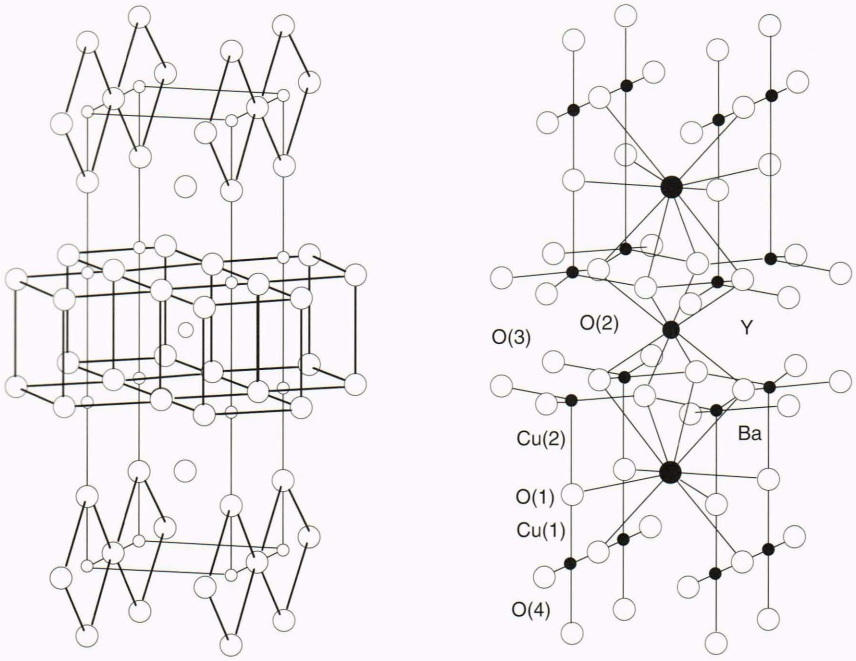

Figure 3. Illustrations of the orthorhombic crystal structure of the YBCO ceramics (e.g., $YBa_2Cu_3O_7$). Here, the crystallographic *c* axis is vertical and the *a* axis is horizontal.

Table 2. Atomic coordinates and site symmetries for $YBa_2Cu_3O_7$ in space group Pmmm.

Atom	Wyckoff notation	Site symmetry	Atomic position
Y	1h	mmm (D_{2h})	1/2, 1/2, 1/2
Ba	2t	mm (C_{2v})	1/2, 1/2, ≈1/5
Cu(1)	2a	mmm (D_{2h})	0, 0, 0
Cu(2)	2q	mm (C_{2v})	0, 0, ≈1/3
O(1)	2q	mm (C_{2v})	0, 0, ≈1/6
O(2)	2q	mm (C_{2v})	1/2, 0, ≈1/3
O(3)	2a	mm (C_{2v})	0, 1/2, ≈1/3
O(4)	1e	mmm (D_{2h})	0, 1/2, 0

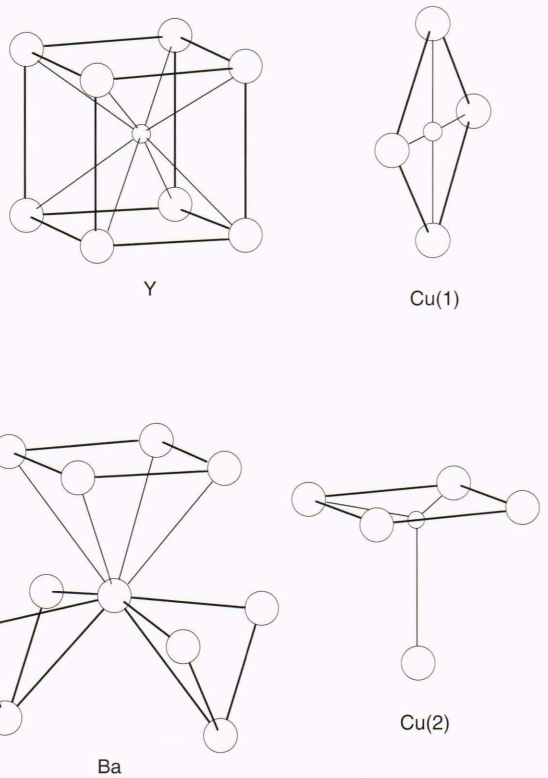

Figure 4. Coordination environments about the Y, Ba, and the two Cu ion sites in the YBCO ceramics (e.g., $YBa_2Cu_3O_7$).

copper on the critical temperature and structural properties both chemically and experimentally intricate.

In what follows, results for some of the chemical substitution data on these high-T_c copper oxide ceramics and their analysis and interpretation are presented. Because the field is rapidly evolving and extensive, a complete presentation of the empirical data or their analysis and interpretation is virtually impossible. Thus, the issues selected here largely reflect personal interest and experimental and theoretical involvement.

SUBSTITUTION AT THE RARE EARTH SITE IN YBCO AND LSCO CERAMICS

YBCO Ceramics

One very early surprise in the crystal chemistry of the YBCO ceramics was the finding that the substitution of several other rare earth ions, R^{3+}, for the Y^{3+} ion in the parent compound did not dramatically alter the superconducting behavior (see, e.g., Ref. 6). In particular, the critical temperature is relatively unaffected by whether the dopant rare earth ion has a magnetic ground state—a surprising result, since magnetism and superconductivity are competitive quantum phenomena. One clear implication of these data, then, is that the portion of the crystal structure near the yttrium ion site is not intimately involved in the superconducting network.

Small but systematic changes, however, occur in the structural and superconducting properties of these materials with substitution by rare earth ions, and of

these, the variation in the *c*-axis length and critical temperature are presented and briefly discussed here. Following the simple ionic model for the bonding in such materials, trends in these two parameters are examined as a function of the ionic radius of the Y^{3+} or rare earth ion. For background, the effect of the number (from 0 to 14) of electrons in the *f* shell on the ionic radius itself for these R^{3+} ions is shown in Figure 5. Clearly, weakly separate (each nearly linear) trends exist for the first and second halves of the series. The Y(III) ion is anomalous in this plot, and expectedly so, given its atypical electronic configuration. For future reference, note that the ionic radius of Y(III) is nearly identical to that of Ho(III).

Figure 6 shows the trend in the *c*-axis length for a series of $RBa_2Cu_3O_3$ ceramics with the ionic radius of the rare earth ion. The approximately linear variation observed immediately suggests that the simple ionic model is a practical first approximation to the chemical bonding at the rare earth site. For added confirmation, note that the data point for the Y-based ceramic takes its "rightful" place near the Ho compound, accentuating the dominant role of ionic size.

Next, Figure 7 shows the correlation between the critical temperature T_c and ionic radius. Although the effect is small (only ≈ 3 K over the series), a nominally linear increase is seen in T_c with the increasing ionic radius of the rare earth ion. The increase in cell volume accompanying the expanded *c*-axis length may lead to an enhanced density of states at the Fermi level and may result in this mild increase in T_c.[7]

LSCO Ceramics

Trends in the *c*-axis length and T_c with the ionic radius of the rare earth ion are now examined for a series of LSCO ceramics (see, e.g., Ref. 8). Here, the problem is a bit more complex. Full substitution for the lanthanum ion by some rare earth ions leads to the adoption of an alternative, nonsuperconducting crystal structure. What has been successfully undertaken is the synthesis of a number of ceramics in which a small fraction (about 10%) of the parent La^{3+} is replaced by another R^{3+} ion. Thus, the rare earth site in the LSCO structure is occupied by La^{3+}, another R^{3+} ion, and Sr^{2+}. Assuming random occupancy, the ionic radius attributed to this site has been calculated as the occupancy-weighted average of the three residing ions. Here, as for the YBCO ceramics, a nominally linear trend in the *c*-axis length with increasing ionic size is observed (Fig. 8). The magnitude of the effect is more dramatic in the LSCO ceramics, however. In fact, on the basis of linear approximations and normali-

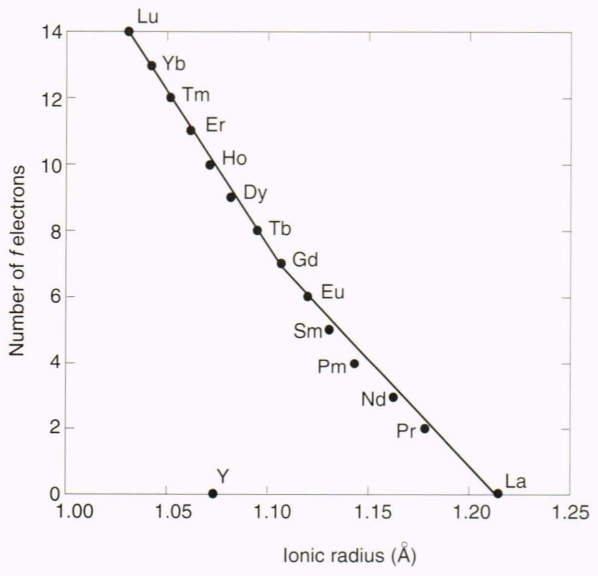

Figure 5. Effect of the number of *f* electrons on the ionic radius of the R^{3+} ion.

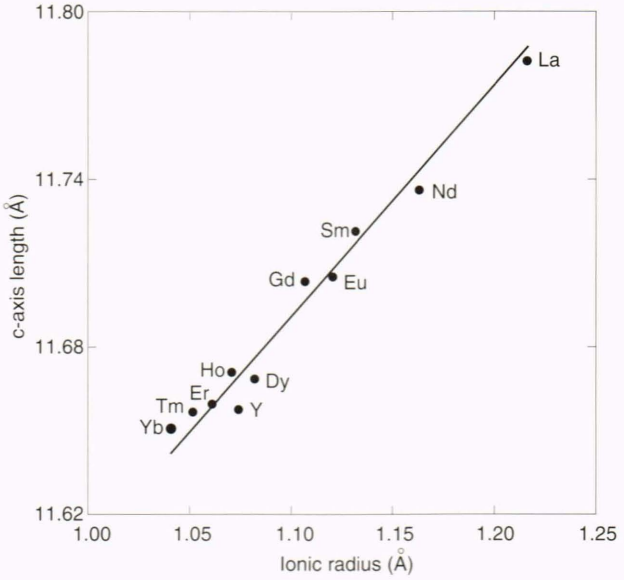

Figure 6. Variation in the *c*-axis length with the ionic radius of the R^{3+} ion in a series of substituted YBCO ceramics.

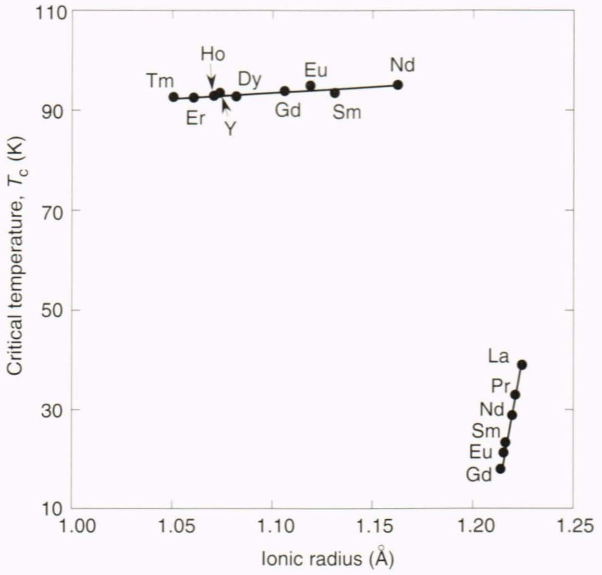

Figure 7. Comparison between the variation in critical temperature T_c and ionic radius for YBCO (upper curve) and LSCO (lower right curve) ceramics.

zation to the number of rare earth sites per cell, the effect in the LSCO ceramics is nearly a factor of four larger than in the YBCO ceramics.

Similarly, the effect on the magnitude of T_c due to substitution at the rare earth site is considerably more dramatic in the LSCO ceramics than in the YBCO ceramics. Figure 7 shows variations in T_c for both families of ceramics. Consistent with Figure 8, the normalized rate of change with ionic radius is nearly an order of magnitude larger for the LSCO ceramics than for the YBCO ceramics.

SUBSTITUTION FOR COPPER IN YBCO AND LSCO CERAMICS

The presence of copper in these ceramics appears to be a crucial element in the realization of high-T_c superconductivity. Expectedly, then, several studies on the substitution of transition metal and nontransition metal ions for copper in these materials have been undertaken.

YBCO Studies

The contribution of plane Cu(2) and chain Cu(1) copper sites to the attainment of the high-T_c in the YBCO ceramics has been and remains a source for theoretical debate and experimentation. The earliest suggestions centered on the chain sites, since this structural element is absent in the lower-T_c LSCO ceramics. Recently, measurements from substitution studies have entered into this controversy, as strong evidence has been presented for preferred substitution in the YBCO structure.

The notion of preferred site substitution follows experimentally from the study of various metal dopants on the superconducting and structural properties of the YBCO ceramics. For example, Figure 9 shows the effect on T_c with Ga^{3+}, Al^{3+}, Zn^{2+}, and Ni^{2+} substitution for copper (see, e.g., Refs. 9–13). Clearly, these results suggest two types of behavior, and it is at the initial stages (the first 3% to 4%) of bulk copper substitution that these two types are differentiated—T_c is virtually unaffected by Ga^{3+} and Al^{3+} substitution and nearly halved for the same level of substitution by Zn^{2+} and Ni^{2+}.

Similarly, Figure 10 shows that in the early stage of Ga^{3+} substitution, for example, the small difference in the crystallographic a and b axes in the orthorhombic phase of the YBCO ceramics is dramatically reduced, and equivalency of the axial lengths, resulting in tetragonal symmetry, is readily achieved. In contrast, the lengths of the a and b axes are virtually unaffected (Fig. 11) by the substitution, for example, of Zn^{2+}. These results are conveniently expressed on a common basis in terms of the effect on the crystallographic strain $\{(b - a)/(b + a)\}$, as shown in Figure 12.

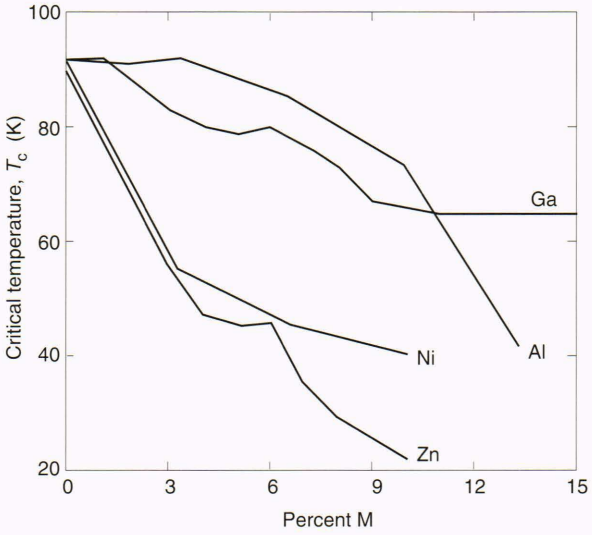

Figure 9. Effect on the critical temperature of metal ion substitution for copper in $YBa(Cu_{1-x}M_x)_3O_y$ ceramics, where M is Al^{3+}, Ga^{3+}, Zn^{2+}, and Ni^{2+}.

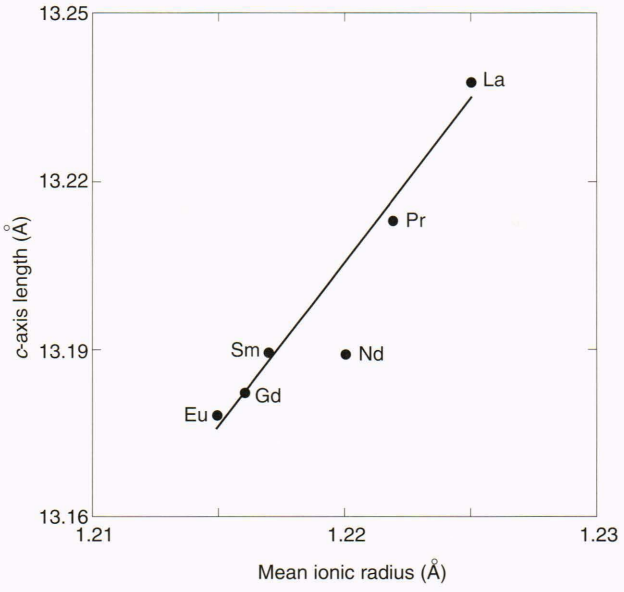

Figure 8. Variation in the c-axis length with ionic radius for a series of LSCO ceramics.

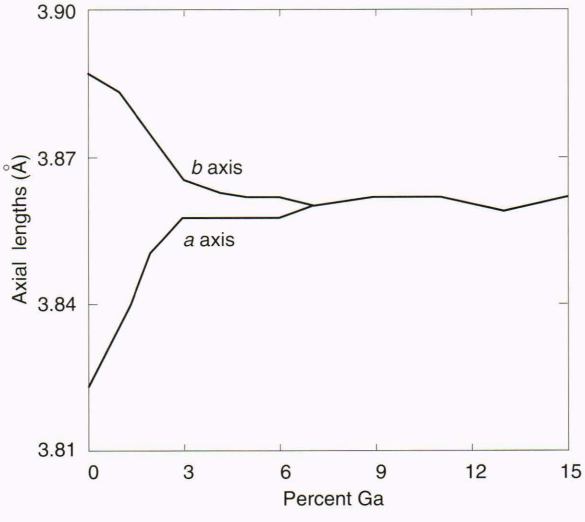

Figure 10. Variation in the length of the a and b cell axes with percent metal substitution for $YBa_2(Cu_{1-x}Ga_x)_3O_y$ ceramics.

It is advantageous here to present an intuitive rationale for the foregoing structural results and to suggest the class of the copper site that the various dopant ions are preferentially occupying. In Figure 3, the topography of the Cu–O chains in the Cu(1) layer and the Cu–O planes in the Cu(2) layers is shown. Obviously, the Cu(1) layer is responsible for the difference in the lengths of the in-plane *a* and *b* axes and the observed orthorhombic symmetry of the unsubstituted ceramic (see, e.g., Refs. 14 and 15). If, however, the oxygen atoms are randomly distributed in this layer, then the *a* and *b* axes would become equal, and tetragonal symmetry would be attained. On the basis of this line of argument, the results presented in Figures 10 and 11 make it likely that the Ga^{3+} ions substitute preferentially at the Cu(1) chain site and the Zn^{2+} ions at the Cu(2) plane site. In addition to this intuitive argument, considerable experimental evidence exists from neutron diffraction data[11,12] for this preferential pattern of substitution. Finally, results for Fe^{3+} and Co^{3+} substitution also strongly suggest preferential occupation of the Cu(1) site.[15]

One immediately notes that the Cu(1) site is selectively occupied by ions with a formal charge of +3 and that the Cu(2) site is selectively occupied by ions with a formal charge of +2. In fact, charge selectivity is probably the direct antecedent of site selectivity in these chemically complex materials.[16] Also, the presence of both open-shell, magnetic—Fe^{3+} and Co^{3+} at the Cu(1) site; Ni^{2+} at the Cu(2) site—and closed-shell, nonmagnetic—Ga^{3+} and Al^{3+} at the Cu(1) site; Zn^{2+} at the Cu(2) site—ions in both limiting regimes suggests that neither exchange nor band filling is the predominant pair-breaking mechanism leading to the loss of superconductivity in these ceramics.

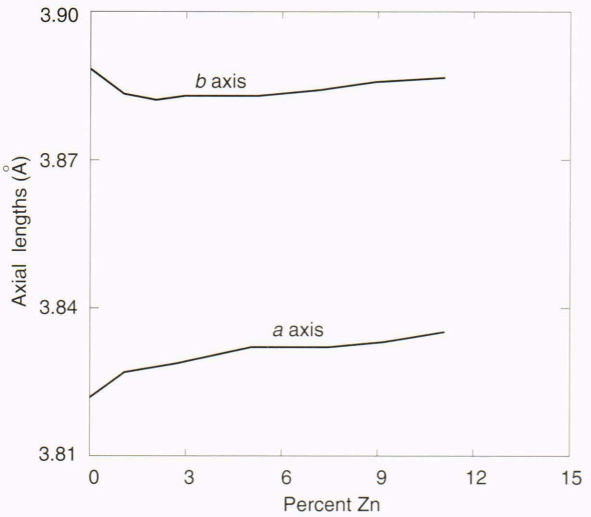

Figure 11. Variation in the length of the *a* and *b* cell axes with percent metal substitution for $YBa_2(Cu_{1-x}Zn_x)_3O_y$ ceramics.

Comparison of Results for YBCO and LSCO Ceramics

For metal ions (Zn^{2+} and Ni^{2+}) with a preference for substitution at the Cu(2) sites in the YBCO structure, it should be interesting to compare the effect of metal doping on T_c with that observed for a comparable level of substitution at the unique copper site in the LSCO structure. The very similar geometry and electronic structure for the CuO_5 planes in the YBCO phase and the CuO_6 planes in the LSCO ceramic seem to ensure that structure and bonding effects ought not severely compromise such a comparison.

Figure 13 compares the combined results for Zn- and Ni-doped YBCO and LSCO ceramics at low substitution

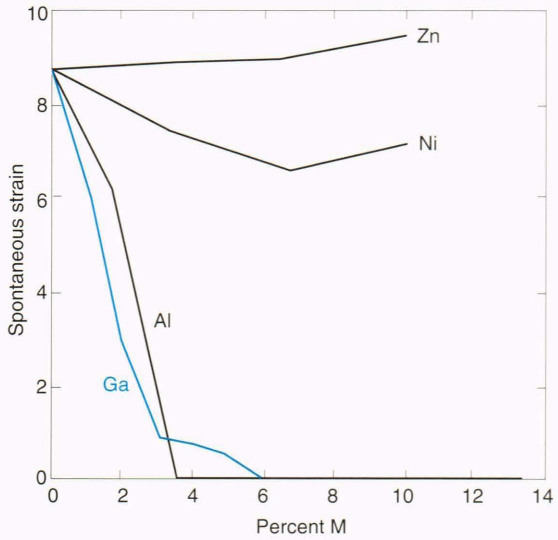

Figure 12. Trend in spontaneous strain with percent metal substitution for $YBa(Cu_{1-x}M_x)_3O_y$ ceramics, where M is Al^{3+}, Ga^{3+}, Zn^{2+}, and Ni^{2+}.

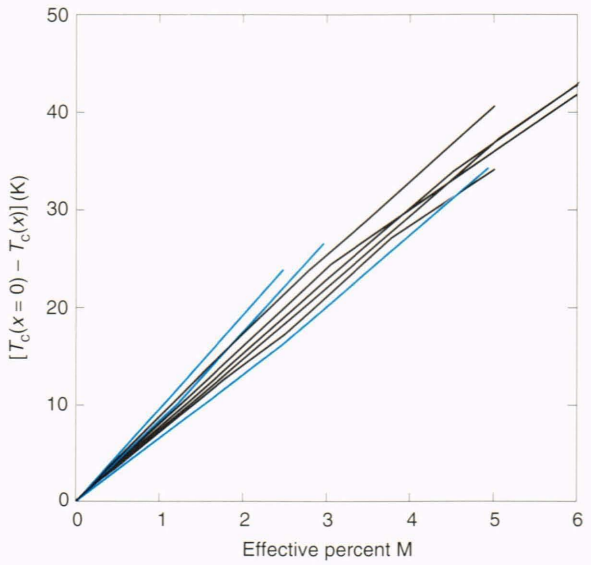

Figure 13. Comparison of $[T_c(x = 0) - T_c(x)]$ versus percent metal substitution in the low doping regime for M = Zn and Ni substitution in YBCO and LSCO ceramics–black curves, $YBa_2(Cu_{1-x}M_x)3O_y$; blue curves, $La_{2-t}Sr_t(Cu_{1-x}M_x)O_z$

levels on a common scale by plotting $[T_c(x = 0) - T_c(x)]$ versus percent metal substitution, with the following amendment: If one assumes strict preferential substitution of Zn^{2+} and Ni^{2+} for the Cu(2) site in the YBCO ceramics, then the metal percentage must be corrected from the bulk value to reflect this selectivity. For a strict preference, the effective metal percentage is 1.5 times that of the bulk value, since only two-thirds of the available Cu sites are being substituted. Given the commonly observed irregularities in the preparation of these materials, the results presented in Figure 13 are considered identical for both Zn and Ni doping and over both families of ceramics. Thus, the same decrease (near 40 K) in T_c for the same limiting percent metal substitution is observed in both the YBCO and LSCO ceramics.

The principal conclusion drawn from this comparison is that the integrity of the planes of Cu–O polyhedra in the YBCO structure is crucial to the achievement of the observed 90 K critical temperature. In short, twice the number of Cu–O planes in the YBCO structure compared with the LSCO motif leads to twice the critical temperature. Such a notion offers many parallels with the recently observed dependence of T_c on the number of Cu–O layers in Tl- and Bi-based oxide superconductors (see, e.g., Ref. 17).

Substitution-Induced Superstructures in Cu(1)-Doped YBCO Ceramics

An interesting (and experimentally frustrating) aspect of the high-temperature superconducting ceramic YBCO is that oxygen variability markedly affects the observed critical temperature and crystal symmetry. At the nominal stoichiometric limits, superconductivity and orthorhombic symmetry are observed at $y = 7$, and semiconductivity and tetragonal symmetry are obtained at $y = 6$. Analysis of high-resolution X-ray and neutron diffraction data has shown that the oxygen atom denoted O(4) in Figure 3 and associated with the Cu(1) layers is almost exclusively the source of this variability. In highly ordered specimens with $y \approx 7$, one-dimensional chains of corner-shared CuO_4 polyhedra propagate along the *b* axis of the orthorhombic cell, as shown in Figure 14A. In crystallographic terms, the O(4) site is fully occupied. At the $y = 6$ limit, both the O(4) and its counterpart site along the *a* axis—denoted O(5)—are devoid of atomic density.

As outlined above, selective substitution at the Cu(1) site by trivalent ions such as Ga^{3+}, Al^{3+}, Fe^{3+}, and Co^{3+} also leads to tetragonal symmetry for doping levels near where 10% to 12% of the Cu(1) sites are substituted. Here, however, the oxygen content is approximately constant, and oxygen site disorder (shown in Fig. 14B) has been commonly thought to account for the tetragonal symmetry. In particular, the tendency of these metal dopants for six-coordination has been seen as a motivation for the rearrangement of the oxygen atoms from that shown in Figure 14A to that shown in Figure 14B.

Considerably less attention has been focused on the role of ordered oxygen superstructures in attaining tetragonal symmetry in these metal-doped ceramics.[18] Exploring how these arrangements could lead to tetragonal symmetry has, however, proved fruitful. To illustrate this train of thought, a reconstructed oxygen site occupancy leading to a (2×2) supercell is shown in Figure 14C. Formally speaking, we see one dopant site (a site of six-coordinate geometry) and three Cu sites (1 two-coordinate and 2 four-coordinate) per cell, which are electrically matched by four equivalent oxygen atoms.

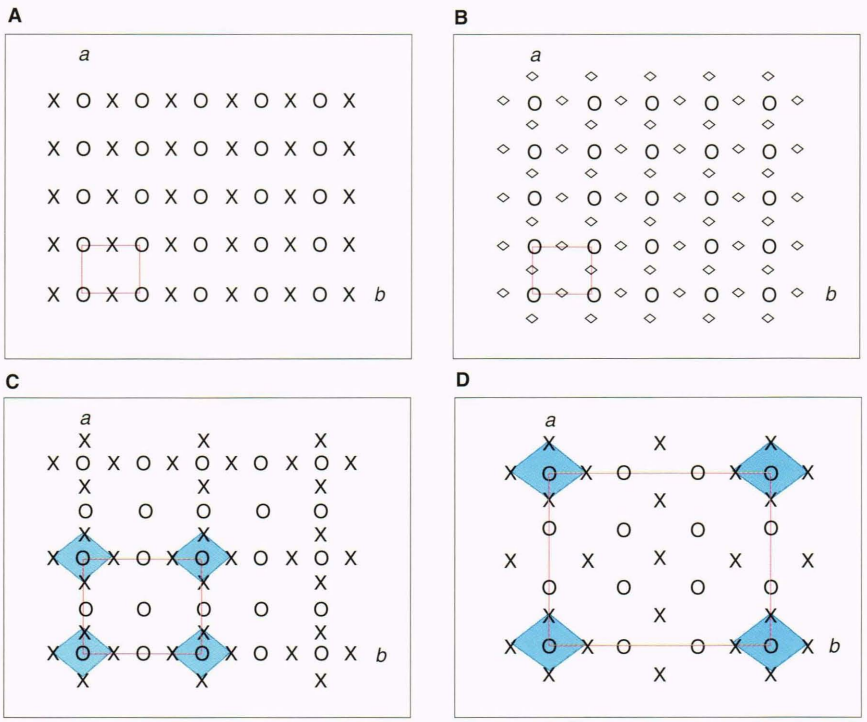

Figure 14. Four alternate, schematic arrangements of the oxygen atoms in the Cu(1)–O layer in the YBCO structure. Copper sites are identified by O's, ordered oxygen atom sites by X's, and disordered oxygen atom sites by diamonds. Oxygen atoms above and below the copper sites complete the coordination polyhedra. **A**. The (1×1) ordered orthorhombic array found in native YBCO. **B**. The (1×1) disordered tetragonal array arising from random site occupancy. **C**. The (2×2) ordered tetragonal supercell with one in four of the metal ion sites showing six-coordination. **D**. The (3×3) ordered tetragonal supercell with one in nine of the metal ion sites showing six-coordination.

Full occupancy of the six-coordinate sites by +3 dopant ions would yield a symmetry transition at 25% substitution of the Cu(1) sites—more than twice the level observed experimentally.

Alternatively, higher-order superstructures can be envisioned, and a reconstruction leading to a (3 × 3) supercell is shown in Figure 14D. Here, one dopant site (a site of six-coordinate geometry) and eight Cu sites exist. In this idealized structure, these eight Cu sites are divided into two types: those along the cell edges, which are five-coordinate (nominally trigonal bipyramidal); and those near the cell center, which are also five-coordinate (nominally square pyramidal). Similarly, two classes of oxygen atom sites exist: those associated with the six-coordinate sites and those lying near the cell center.

The explicit advantages of the (3 × 3) superstructure shown in Figure 14D are twofold: (1) full occupancy of the six-coordinate sites by dopant ions implies an orthorhombic-to-tetragonal transition at 11.1% (one in nine) substitution of the Cu(1) sites, in accord with experimental results; and (2) this (3 × 3) supercell minimizes the number of repulsive oxygen–atom oxygen–atom nearest-neighbor interactions to those associated with the dopant sites.

To emulate the substitution of cations, Madelung energies (the electrostatic contribution to crystal cohesion) for various ionic charges at the substitution site have been evaluated and the results presented in Figure 15. At the critical concentration (≈11%) of +3 dopant in the Cu(1)–O plane leading to tetragonal symmetry, the (3 × 3) ordered supercell is significantly favored over the (1 × 1) disordered array and the (2 × 2) ordered supercell. Thus, a (3 × 3) ordered oxygen atom reconstruction may have a fundamental role in the achievement of tetragonal symmetry when +3 dopants are selectively substituted into the Cu(1) site of the YBCO structure.

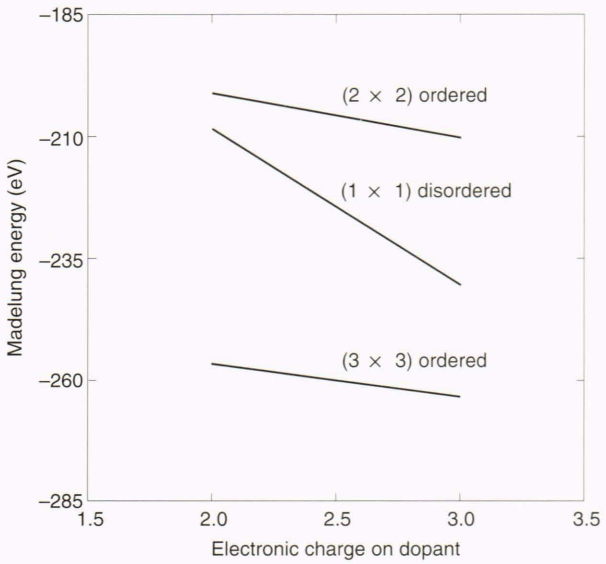

Figure 15. Results of Madelung energy calculations for three of the supercell models shown in Figure 14 with various charges on the dopant ion.

REFERENCES

[1] Bednorz, J. G., and Muller, K. A., "Possible High T_c Superconductivity in the BaLaCuO System," *Z. Phys. B* **64**, 189–193 (1986).

[2] Wu, M. K., Ashburn, J. R., Torng, C. J., Hor, P. H., Meng, R. L., et al., "Superconductivity at 93 K in a New Mixed-Phase YBaCuO Compound System at Ambient Pressure," *Phys. Rev. Lett.* **58**, 908–910 (1987).

[3] Jorgensen, J. D., Schuttler, H.–B., Hinks, D. G., Capone, D. W., Zhang, K., et al., "Lattice Instability and High T_c Superconductivity in $La_{2-x}Ba_xCuO_4$," *Phys. Rev. Lett.* **58**, 1024–1027 (1987).

[4] Beno, M. A., Soderholm, L., Capone, D. W., Hinks, D. G., Jorgensen, J. D., et al., "Structure of the Single-Phase High-Temperature Superconductor $YBa_2Cu_3O_{7-x}$," *Appl. Phys. Lett.* **51**, 57–59 (1987).

[5] Greeden, J. E., O'Reilly, A. H., and Stager, C. V., "Oxygen Ordering in the Crystal Structure of the 93 K Superconductor $YBa_2Cu_3O_7$ Using Powder Neutron Diffraction at 298 and 79.5 K," *Phys. Rev. B* **35**, 8770–8773 (1987).

[6] Tarascon, J. M., McKinnon, W. R., Greene, L. H., Hull, G. W., and Vogel, E. M., "Oxygen and Rare-Earth Doping of the 90-K Superconducting Perovskite $YBa_2Cu_3M_xO_{7-x}$," *Phys. Rev. B* **36**, 226–234 (1987).

[7] Kistenmacher, T. J., "Effect of the Rare-Earth Ion R on Structure and Superconductivity in High-T_c $RBa_2Cu_3O_y$ Ceramics," *Solid State Commun.* **65**, 981–985 (1988).

[8] Tarascon, J. M., Greene, L. H., Barboux, P., McKinnon, W. R., Hull, G. W., et al., "3d-Doping of High-Temperature Superconducting Perovskites La–Sr–Cu–O and Y–Ba–Cu–O," *Phys. Rev. B* **36**, 8393–8400 (1987).

[9] Tarascon, J. M., Barboux, P., Miceli, P. F., Greene, L. H., Hull, G. W., et al., "Structure and Physical Properties of the Metal (M) Substituted $YBa_2Cu_{3-x}M_xO_{7-y}$ Perovskites," *Phys. Rev. B* **37**, 7458–7469 (1988).

[10] Xiao, G., Streitz, F. H., Gavrin, A., Du, Y.–W., and Chien, C. L., "Effect of Transition Metal Elements on Superconductivity of Y–Ba–Cu–O," *Phys. Rev. B* **35**, 8782–8784 (1987).

[11] Xiao, G., Cieplak, M. Z., Musser, D., Gavrin, A., Streitz, F. H., et al., "Significance of Plane versus Chain Sites in High-Temperature Oxide Superconductors," *Nature (London)* **332**, 238–240 (1988).

[12] Xiao, G., Cieplak, M. Z., Gavrin, A., Streitz, F. H., Bakhshai, A., et al., "High-Temperature Superconductivity in Tetragonal Perovskite Structures: Is Oxygen-Vacancy Order Important?" *Phys. Rev. Lett.* **60**, 1446–1449 (1988).

[13] Kistenmacher, T. J., Bryden, W. A., Morgan, J. S., Moorjani, K., Du, Y.–W., et al., "Stabilization of the Tetragonal Phase and Superconducting Behavior in $RBa_2(Cu_{1-x}Fe_x)_3O_y$: R = Y, Gd; $0 < x < 0.15$," *Phys. Rev. B* **36**, 8877–8880 (1987).

[14] Kistenmacher, T. J., "Oxygen Content and Site Distribution in High-T_c Superconducting $YBa_2Cu_3O_y$ Ceramics," *Inorg. Chem.* **26**, 3649–3650 (1987).

[15] Kistenmacher, T. J., "Mapping the Orthorhombic-to-Tetragonal Transition at Ambient Temperature in $YBa_2Cu_3O_y$ Ceramics," *J. Appl. Phys.* **64**, 5067–5070 (1988).

[16] Kistenmacher, T. J., "Substitution for Copper in $YBa_2Cu_3O_y$: The First 3%," *Phys. Rev. B* **38**, 8862–8867 (1988).

[17] Sleight, A. W., "Chemistry of High-Temperature Superconductors," *Science* **242**, 1519–1527 (1988).

[18] Kistenmacher, T. J., "Substitution-Induced Superstructures in Cu(1)-Doped $YBa_2(Cu_{1-x}M_x)_3O_y$ Ceramics (M = Trivalent Cation)," *Phys. Rev. B* **39**, 12279–12282 (1989).

THE AUTHOR

THOMAS J. KISTENMACHER is a Principal Professional Staff chemist in APL's Milton S. Eisenhower Research Center. He obtained a B.S. degree in chemistry from Iowa State University and M.S. and Ph.D. degrees in chemistry from the University of Illinois. During 1969–71, he was a Junior Fellow in chemical physics at the California Institute of Technology. During 1971–82, he served on the faculties of The Johns Hopkins University and the California Institute of Technology. Dr. Kistenmacher joined APL in 1982 as a member of the Microwave Physics Group. In 1984, he became a member of the Materials Science Group, where his current research interests include crystalline structure and structure–physical property relationships in highly conductive organic solids, local structure and magnetic properties of amorphous thin films and multilayers, the elucidation of structural models for icosahedral materials, the structural basis for high-T_c oxide ceramics, and large bandgap metal-nitride semiconductors.